A Generalized Method for Deriving the Space-Domain Green's Function in a Shielded, Multilayer Substrate Structure with Applications to MIS Slow-Wave Transmission Lines

THOMAS G. LIVERNOIS AND PISTI B. KATEHI, MEMBER, IEEE

Abstract —**An efficient technique for deriving the space-domain Green's function due to an arbitrarily oriented current in shielded, multilayer substrate structures is presented. The derived Green's function is then used to find the dispersion characteristics of single and symmetric coupled line MIS slow-wave structures. These results are compared to published theoretical and experimental data to verify the theory presented.**

I. INTRODUCTION

THERE HAS been considerable effort devoted to the design and realization of monolithic microwave integrated circuits (MMIC's) for use in the $f > 20$ GHz region [1]. Once fabricated, monolithic circuits are very difficult to tune for optimum performance and this is a major drawback [1], [2]. Accurate theoretical models of MMIC components are required so that device performance can be predicted confidently, thus avoiding a time-consuming and costly production cycle. Such characterization requires a mathematically rigorous solution for the fields in a particular structure. The use of a Green's function is, therefore, appropriate. Generalized techniques for deriving the spectral-domain or space-domain Green's function for multilayer substrates have been given, but only current densities which are parallel to the layer interfaces are allowed in these approaches [3]–[5]. These techniques find useful application in the analysis of planar integrated circuits and antennas embedded in layered regions. In [6], the Green's function for a rectangular waveguide filled with two dielectrics is given. The inhomogeneous system of equations encountered in [6] increases substantially with the number of layers, thus making the required algebra difficult and time consuming. It is the purpose of this paper to outline a method for deriving the space-domain Green's function for an arbitrarily oriented current in a rectangular waveguide inhomogeneously filled with an arbitrary number of lossy, isotropic dielectric slabs. The approach given here is based on the principle of scattering superposition combined with appropriately chosen magnetic and electric vector potentials. The major advantages of this work are (i) the developed method for evaluating the Green's function can be applied to a current of any orientation and (ii) the solution for unknown-amplitude coefficients always reduces to having to solve 2×2 inhomogeneous sets of equations, regardless of the number of dielectric layers. The scattering parameters of planar stripline discontinuities occurring in shielded, multilayer substrate circuitry may be numerically characterized by following the procedure given in [7] combined with the Green's function obtained here. Research in this direction is proceeding and much remains to be done [7]–[10].

MIS slow-wave structures have been studied by several researchers and are used widely in related MIC's. The slowing effect can be applied to many devices, among them delay lines, phase shifters, and tunable filters. Both single and coupled line geometries have been analyzed using full-wave techniques [11]–[15]. The two rigorous methods which have been applied to these structures in the past, namely spectral-domain analysis and finite element method, can be somewhat cumbersome to work with. The spectral approach requires the use of current basis functions which have well-behaved Fourier transforms, and the finite element method sometimes yields spurious mode results which are difficult to interpret. The present technique, which will be discussed in more detail later, suffers from neither of these drawbacks. The Green's function for an inhomogeneously filled rectangular waveguide derived using the present theory is used to find dispersion characteristics for various slow-wave transmission lines. These results are compared to published theoretical and experi-

Manuscript received February 16, 1989; revised June 26, 1989. This work was supported by the National Science Foundation under Grant ECS-8602530.

The authors are with the Radiation Laboratory, Department of Electrical Engineering and Computer Science, University of Michigan, Ann Arbor, MI 48109-2122.

IEEE Log Number 8930662.

0018-9480/89/1100-1761$01.00 ©1989 IEEE

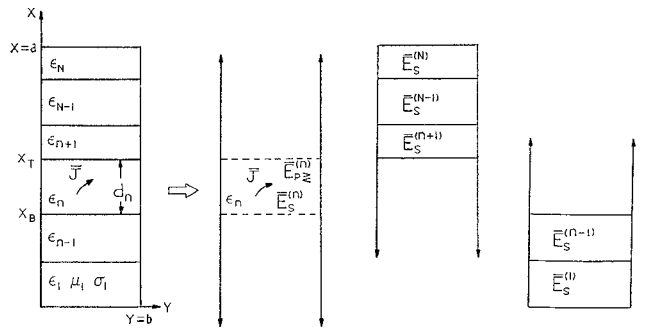

Fig. 1. Representation of inhomogeneously loaded rectangular waveguide as the superposition of parallel-plate structures.

ment results [16] to establish the validity and usefulness of the analytical method given in this paper.

II. Theory

The principle of scattering superposition was first discussed by Tai [17] and recently was used to present the space-domain Green's function for an inhomogeneously filled waveguide [6]. In addition to being a somewhat tedious approach, the vector potentials used in [6] to generate the electromagnetic fields are the $\boldsymbol{M}$, $\boldsymbol{N}$, and $\boldsymbol{L}$ functions described in [17]. The magnetic and electric vector potentials, $\boldsymbol{A}$ and $\boldsymbol{F}$, respectively, [18] are used in the present work and the electromagnetic fields are obtained as

$$\boldsymbol{E} = \frac{1}{\epsilon}\nabla \times \boldsymbol{F} - j\omega\boldsymbol{A} + \frac{1}{j\omega\mu\epsilon}\nabla\nabla\cdot\boldsymbol{A} \tag{1a}$$

$$\boldsymbol{H} = \frac{1}{\mu}\nabla \times \boldsymbol{A} + j\omega\boldsymbol{F} - \frac{1}{j\omega\mu\epsilon}\nabla\nabla\cdot\boldsymbol{F}. \tag{1b}$$

Fig. 1 shows an infinitesimal current source located within a rectangular waveguide that is inhomogeneously loaded with N isotropic, lossy dielectric layers. This waveguide is represented as the superposition of three parallel-plate structures. We begin by considering the total field maintained by $\boldsymbol{J}$ as a superposition of primary and scattered fields.

Primary electromagnetic fields are generated from the primary vector potentials $\boldsymbol{A}_p$ and $\boldsymbol{F}_p$, and must satisfy only the boundary conditions imposed by the equivalent parallel-plate waveguide containing $\boldsymbol{J}$. In general, $\boldsymbol{J}$ will have one component normal to layer interfaces, $\hat{a}_n J_n$, and one component tangential to them, $\hat{a}_t J_t$. For an arbitrarily oriented electric current in the nth layer, the relevant primary field boundary conditions at the source are

$$\hat{a}_n \times (\boldsymbol{E}_{p>} - \boldsymbol{E}_{p<}) = 0 \tag{2a}$$

$$\hat{a}_n \times (\boldsymbol{H}_{p>} - \boldsymbol{H}_{p<}) = \hat{a}_t J_t \tag{2b}$$

$$\nabla^2 \boldsymbol{A}_p + k^2 \boldsymbol{A}_p = -\mu \hat{a}_n J_n \tag{2c}$$

where the $(\gtrless)$ represents $(x \gtrless x')$. Separate application of equations (2) for each component of $\boldsymbol{J}$ yields the desired primary field terms. Scattered fields in the nth layer are derived from $\boldsymbol{A}_s^{(n)}$ and $\boldsymbol{F}_s^{(n)}$ where

$$\nabla^2 \boldsymbol{A}_s^{(n)} + k^2 \boldsymbol{A}_s^{(n)} = 0 \tag{3a}$$

$$\nabla^2 \boldsymbol{F}_s^{(n)} + k^2 \boldsymbol{F}_s^{(n)} = 0, \qquad n = 1,2,\cdots,N. \tag{3b}$$

$\boldsymbol{A}_s^{(n)}$ and $\boldsymbol{F}_s^{(n)}$ must satisfy the boundary conditions imposed by the shorted, dielectric-filled parallel-plate structures. Primary fields result directly from $\boldsymbol{J}$ and exist only in the layer where $\boldsymbol{J}$ is nonzero. The scattered fields result when the dielectric layers and conducting walls are added to the primary structure.

The total field in any layer maintained by $\boldsymbol{J}$ must satisfy the usual source and interface boundary conditions. Both primary and scattered potentials are chosen to be x-directed so that the resulting LSM and LSE fields decouple [3]. The proper eigenfunction expansions for these fields may now be deduced. The primary potentials are

$$A_{x_p} = \frac{1}{2\pi}\int_{-\infty}^{\infty} dk_z \sum_m \tilde{a}_{x_m}(k_z|x, y|x', y')\, e^{-jk_z(z-z')} \tag{4a}$$

$$F_{x_p} = \frac{1}{2\pi}\int_{-\infty}^{\infty} dk_z \sum_m \tilde{f}_{x_m}(k_z|x, y|x', y')\, e^{-jk_z(z-z')}. \tag{4b}$$

The scattered potentials are written as

$$A_{x_s}^{(i)} = \frac{1}{2\pi}\int_{-\infty}^{\infty} dk_z \sum_m A_m^{(l)} \tilde{a}_{x_m}^{(i)}(k_z|x, y|x', y')\, e^{-jk_z(z-z')} \tag{5a}$$

$$F_{x_s}^{(i)} = \frac{1}{2\pi}\int_{-\infty}^{\infty} dk_z \sum_m F_m^{(l)} \tilde{f}_{x_m}^{(i)}(k_z|x, y|x', y')\, e^{-jk_z(z-z')} \tag{5b}$$

where i denotes the layer and

$$\begin{aligned} &l = N, && i = n+1,\cdots,N \\ &l = n, && \text{when } i = n \\ &l = 1, && i = 1,\cdots,n-1. \end{aligned}$$

$\boldsymbol{J}$ is assumed to be in the nth layer and $A_m^{(l)}$ and $F_m^{(l)}$ are the unknown scattered vector potential amplitude coefficients in the lth layer, where $l = 1, n, N$. All boundary conditions in the rectangular waveguide are satisfied except those at $x = x_T$ and $x = x_B$. These boundary conditions are written as

$$E_{y_p}^{(n)}{}_{\gtrless} + E_{y_s}^{(n)} = E_{y_s}^{(n\pm1)} \tag{6a}$$

$$E_{z_p}^{(n)}{}_{\gtrless} + E_{z_s}^{(n)} = E_{z_s}^{(n\pm1)} \tag{6b}$$

$$H_{y_p}^{(n)}{}_{\gtrless} + H_{y_s}^{(n)} = H_{y_s}^{(n\pm1)} \tag{6c}$$

$$H_{z_p}^{(n)}{}_{\gtrless} + H_{z_s}^{(n)} = H_{z_s}^{(n\pm1)} \tag{6d}$$

where the $(\gtrless)$ and $(\pm)$ are for $\begin{pmatrix} x = x_T \\ x = x_B \end{pmatrix}$. The primary fields are obtained from (1) with $\boldsymbol{A} = \hat{a}_x A_{x_p}$ and $\boldsymbol{F} = \hat{a}_x F_{x_p}$. The scattered fields are obtained similarly with $\boldsymbol{A} = \hat{a}_x A_{x_s}^{(i)}$ and $\boldsymbol{F} = \hat{a}_x F_{x_s}^{(i)}$, $i = 1,2\cdots,N$. Since LSM and LSE fields are orthogonal [18], the inhomogeneous 8×8 set of equations resulting from (6) decouples into four inhomogeneous 2×2 sets of equations. Solving for $A_m^{(N)}$, $F_m^{(N)}$, $A_m^{(n)}$, $F_m^{(n)}$, $A_m^{(1)}$, and $F_m^{(1)}$ and combining with (1a), (4), and (5) yields the integral representation of the electric field any-

where in the waveguide:

$$\boldsymbol{E}(x, y, z|x', y', z') = \frac{1}{2\pi}\int_{-\infty}^{\infty} dk_z \sum_m \hat{a}_e \tilde{e}_m \cdot (k_z|x, y|x', y') e^{-jk_z(z-z')} \quad (7)$$

where $\hat{a}_e$ is a unit vector along the direction of the electric field.

The remaining task is to complete the inverse Fourier transform of (7). This integral may be evaluated via the calculus of residues since no branch points exist in the integrand. In general, $\tilde{e}_m$ is made up of LSM and LSE contributions. For both LSM and LSE modes, the inversion contour in the k_z plane is closed in the lower half for $z < z'$ and in the upper half for $z > z'$. The distribution of poles in he k_z plane is symmetric about the origin. Completing the inverse transform of (7) for each component of the electric field yields the dyadic Green's function:

$$\bar{\bar{G}}_E(x|x', y|y', z|z') = \sum_n \sum_m \bar{\bar{G}}_{nm}^{\mathrm{LSM}} + \sum_p \sum_m \bar{\bar{G}}_{pm}^{\mathrm{LSE}} \quad (8a)$$

where the electric field due to an arbitrary electric current is now given by

$$\boldsymbol{E}(x, y, z) = \iiint \bar{\bar{G}}_E(x, y, z|x', y', z') \cdot \boldsymbol{J}(x', y', z')\, dx'\, dy'\, dz'. \quad (8b)$$

Equations (8a) and (8b) give the space-domain Green's function, which is useful for three-dimensional problems. For the analysis of two-dimensional problems, fields described in the form of (7) are appropriate. The method presented here may also be applied to structures containing an arbitrary number of electric and magnetic sources.

III. Dispersion Analysis

The shielded microstrip structures illustrated in Fig. 2 are characterized by their respective coupled integral equations:

$$\begin{bmatrix} G_{yy} & G_{yz} \\ G_{zy} & G_{zz} \end{bmatrix} * \begin{bmatrix} J_y \\ J_z \end{bmatrix} = \begin{bmatrix} E_y \\ E_z \end{bmatrix}. \quad (9)$$

The components of the Green's matrices are derived in integral form for a three-layer waveguide, as in (7), with the infinitesimal source located in region (2). The expansions for J_y and J_z are chosen to satisfy their respective edge conditions [19]. The convolution integrals resulting from (9) are evaluated in closed form. Using one expansion term for J_y and J_z and applying the Galerkin's procedure to (9) shows

$$\begin{bmatrix} \sum_{\substack{m=1 \\ \text{odd}}}^{M} P_{1m} & \sum_{\substack{m=1 \\ \text{odd}}}^{M} Q_{1m} \\ \sum_{\substack{m=1 \\ \text{odd}}}^{M} S_{1m} & \sum_{\substack{m=1 \\ \text{odd}}}^{M} U_{1m} \end{bmatrix} \begin{bmatrix} c_1 \\ d_1 \end{bmatrix} = \begin{bmatrix} 0 \\ 0 \end{bmatrix} \quad (10)$$

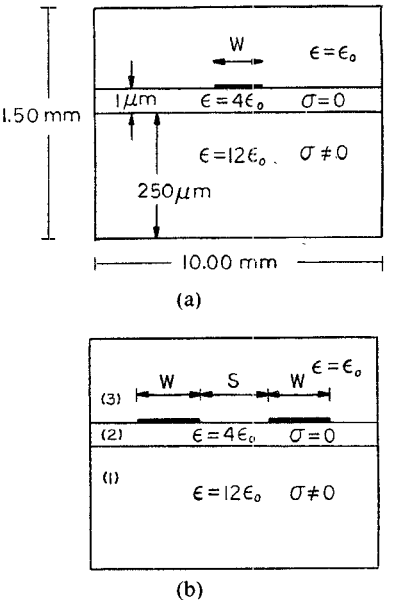

Fig. 2. Geometry of single and coupled microstrip slow-wave structures.

where c_1 is the unknown amplitude coefficient for the first expansion term of J_y, and d_1 similarly results from J_z.

For both single and coupled line structures the expressions for P_{1m}, Q_{1m}, S_{1m}, and U_{1m} are relatively simple combinations of Bessel and trigonometric functions. These are given in the Appendix. Setting the determinant of the current amplitude matrix to zero and solving for its roots yields the complex microstrip propagation constant $k_z = \beta - j\alpha$ for the respective structures.

IV. Numerical Results

The dispersion characteristics given in this section are for the single and coupled strip MIS structures illustrated in Fig. 2. The pertinent dimensions are also given there. Region 1 is the conducting Si substrate with $\epsilon_{r1} = 12$ and region 2 is the SiO_2 insulating region with $\epsilon_{r2} = 4$. The effect of the induced conduction current is incorporated into a complex permittivity in region 1. The normalized wavelength and the attenuation constant for different cases are plotted in Figs. 3–10. Good convergence was obtained using one expansion term for the microstrip current components and $M = 501$ in the four truncated series in (10). Roots of the matrix were found using Mueller's method with deflation.

Figs. 3 and 4 show a comparison of phase and attenuation constants between this theory, spectral analysis, finite element method, and experimental results for a narrow single MIS line with $w = 160$ μm. Dispersion characteristics for a wide single MIS line with $w = 600$ μm are compared with other full-wave methods, parallel-plate model results, and experimental results in Figs. 5 and 6. Good agreement between this theory, experiment, and other full-wave methods for λ/λ_0 and α is found in all cases studied for the single MIS line with $w = 160$ μm. Results for the wider strip, $w = 600$ μm, show discrepancies between his theory and the spectral-domain approach

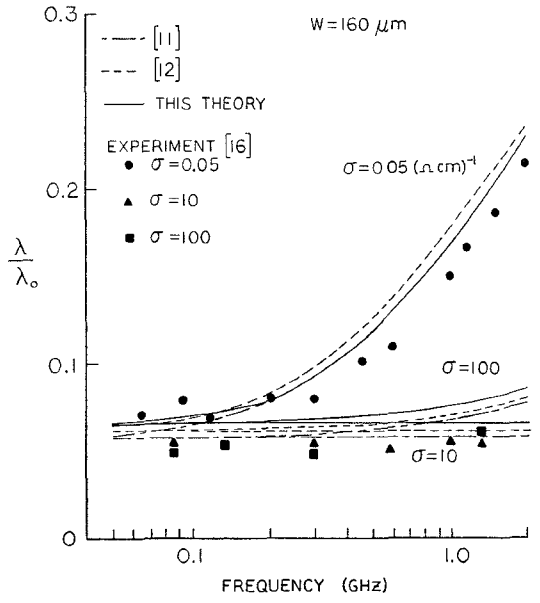

Fig. 3. Comparison of normalized wavelength for single microstrip ($w = 160$ μm) with spectral-domain analysis [11], finite element method [12], and experimental results [16].

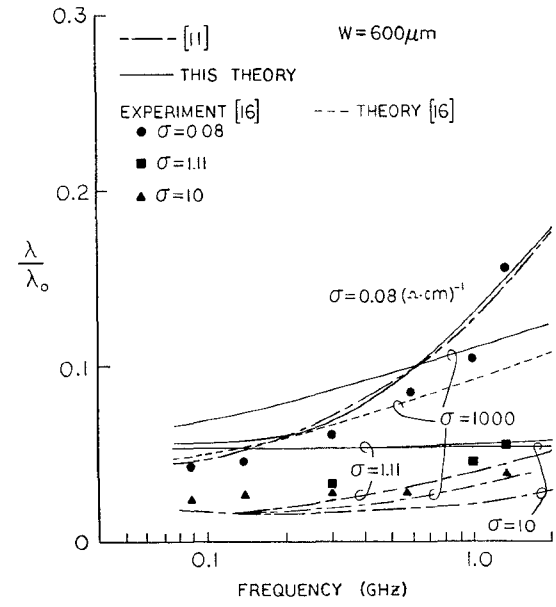

Fig. 5. Comparison of normalized wavelength for single microstrip ($w = 600$ μm) with spectral-domain analysis [11], experimental results [16], and parallel-plate model [16].

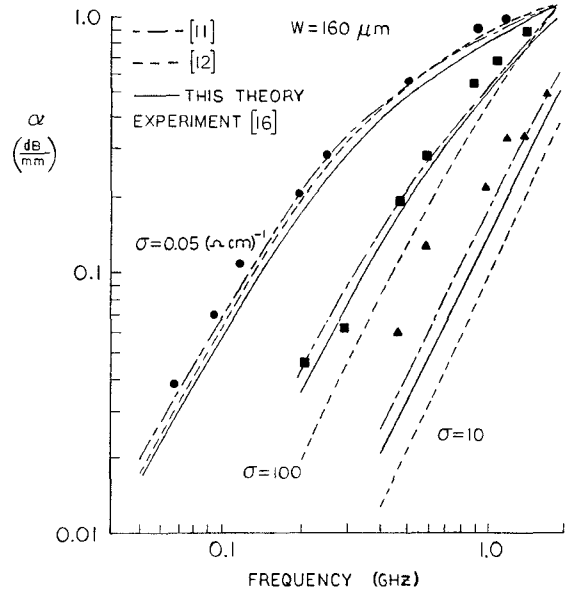

Fig. 4. Comparison of attenuation constant for single microstrip ($w = 160$ μm) with spectral-domain analysis [11], finite element method [12], and experimental results [16].

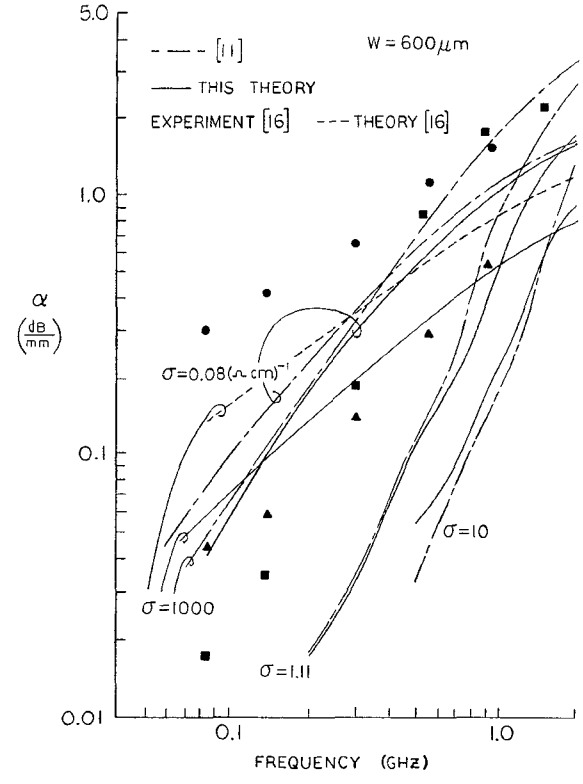

Fig. 6. Comparison of attenuation constant for single microstrip ($w = 600$ μm) with spectral-domain analysis [11], experimental results [16], and parallel-plate model [16].

for larger substrate conductivities. For the case $\sigma = 1000$ and $f = 1$ GHz, the spectral analysis finds a very low normalized wavelength of about 0.04. This value is unacceptable considering that the Si substrate is five skin depths thick. As a result, the electromagnetic fields are virtually shielded from the semiconducting layer. This drives the line into the skin effect and not the slow-wave mode. Results derived by the method presented in this paper indicate such a tendency. Curves generated from the parallel-plate analysis (applicable to wide microstrips) [16] are also plotted in Figs. 5 and 6 and are in agreement with our theoretical data.

Discrepancies between this theory and experimental results are also evident for the wide-strip case. Consequently, to verify the accuracy of this approach when applied to wide strips, a comparison of normalized dominant mode phase constant for the $w/h = 2$ structure analyzed in [20] was made. Virtual exact agreement was found for the

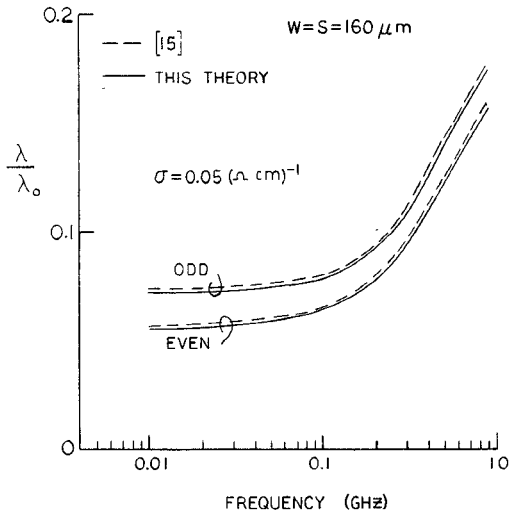

Fig. 7. Comparison of normalized wavelength for even- and odd-mode excitation of coupled microstrip lines with spectral-domain analysis [15].

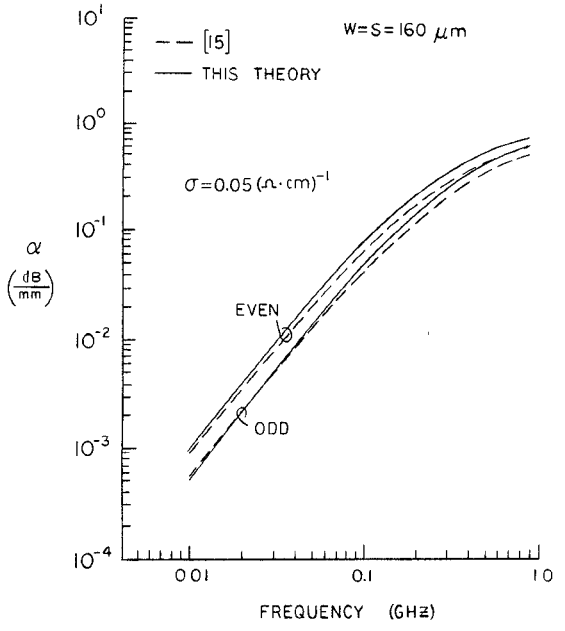

Fig. 8. Comparison of attenuation constant for even- and odd-mode excitation of coupled microstrip lines with spectral-domain analysis [15].

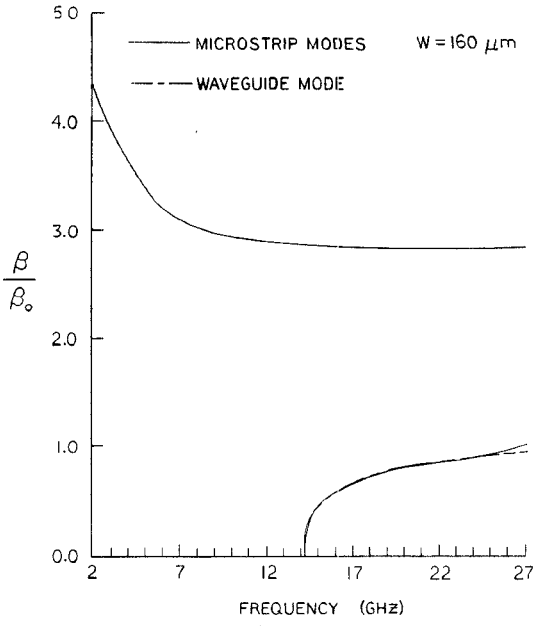

Fig. 9. Frequency–phase constant characteristics or first two modes of single microstrip and dominant mode of inhomogeneously filled waveguide.

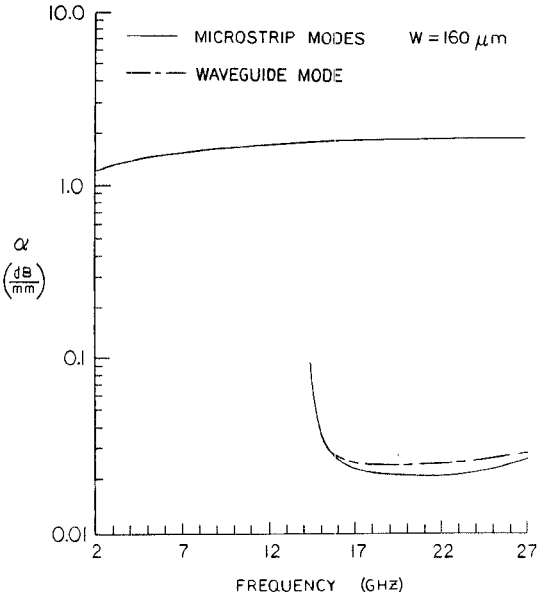

Fig. 10. Frequency–attenuation constant characteristics for first two modes of single microstrip and dominant mode of inhomogeneously filled waveguide.

entire frequency range studied (1–100 GHz). Phase and attenuation constants for the coupled line MIS structure are shown in Figs. 7 and 8. The propagation characteristics found using this theory compare very well with the spectral analysis results. Fig. 7 shows λ/λ_0 for even- and odd-mode excitation and Fig. 8 shows the comparison of α for even- and odd-mode excitation.

The last two sets of data, Figs. 9 and 10, show the frequency dependence of phase and attenuation constants for the first two modes of the single MIS line with $w = 160$ μm and the dominant mode of the rectangular waveguide (no strip). These results show a clear correlation between the second microstrip mode and dominant waveguide mode dispersion characteristics over the entire frequency range studied. This phenomenon was also reported in [20] for a lossless dielectric substrate.

The amount of time required to find a solution to the determinantal equation (10) ranged from 55 seconds for small values of the loss tangent in region (1) (i.e., $\sigma = 0.05$, $f = 1$ GHz) to 285 seconds for larger values (i.e., $\sigma = 1000$, $f = 0.5$ GHz). These calculations were done on a personal computer.

V. Conclusion

This paper has presented a simple, efficient technique for deriving a physically appealing space-domain Green's function in a shielded layered region containing an arbitrary number of magnetic and/or electric sources. Obtain-

ing unknown amplitude coefficients reduces to the solution of 2×2 inhomogeneous sets of equations, depending on the number of different layers containing sources. The Green's function for an inhomogeneously filled waveguide was derived and used to find dispersion characteristics for various MIS slow-wave structures. The corresponding characteristic equations are given in an appendix. The accuracy of the results was verified by a comparison with other published data, thus establishing the validity of the theory presented.

Appendix
Expressions for P_{1m}, Q_{1m}, S_{1m}, and U_{1m} for Single and Coupled Lines

A. Single MIS Line

$$P_{1m} = -C_1C_3^2K_1$$

$$U_{1m} = C_1C_2^2K_2$$

$$Q_{1m} = S_{1m} = C_1C_2C_3K_3.$$

B. Coupled MIS Lines

Even mode:

$$P_{1m} = -C_1C_3^2C_4^2K_1$$

$$U_{1m} = C_1C_2^2C_4^2K_2$$

$$Q_{1m} = S_{1m} = C_1C_2C_3C_4^2K_3.$$

Odd mode:

$$P_{1m} = -C_1C_3^2C_5^2K_1$$

$$U_{1m} = C_1C_2^2C_5^2K_2$$

$$Q_{1m} = S_{1m} = C_1C_2C_3C_5^2K_3$$

where

$$C_1 = \frac{j2\omega\mu_0}{b\left[\left(\frac{m\pi}{b}\right)^2 + k_z^2\right]}$$

$$C_2 = J_0\left(\frac{m\pi w}{2b}\right)$$

$$C_3 = \frac{\sin\left(\frac{m\pi w}{2b}\right)}{\left[\left(\frac{m\pi w}{2b}\right)^2 - \pi^2\right]}$$

$$C_4 = \cos\left[\frac{m\pi}{2b}(s+w)\right]$$

$$C_5 = \sin\left[\frac{m\pi}{2b}(s+w)\right]$$

and

$$K_1 = \left[\left(\frac{k_x^{(2)}k_x^{(3)}\left(\frac{m\pi}{b}\right)^2}{k_0^2}\right)T_{\mathrm{LSM}} - k_z^2T_{\mathrm{LSE}}\right]$$

$$K_2 = \left[\left(\frac{k_x^{(2)}k_x^{(3)}k_z^2}{k_0^2}\right)T_{\mathrm{LSM}} - \left(\frac{m\pi}{b}\right)^2T_{\mathrm{LSE}}\right]$$

$$K_3 = \left(\frac{m\pi}{b}\right)k_z\left[\left(\frac{k_x^{(2)}k_x^{(3)}}{k_0^2}\right)T_{\mathrm{LSM}} + T_{\mathrm{LSE}}\right]$$

$$T_{\mathrm{LSM}} = \frac{N_{\mathrm{LSM}}}{D_{\mathrm{LSM}}}$$

$$T_{\mathrm{LSE}} = \frac{N_{\mathrm{LSE}}}{D_{\mathrm{LSE}}}$$

$$N_{\mathrm{LSM}} = \tan\left(k_x^{(3)}d_3\right)\left[\epsilon_{r_1}k_x^{(2)}\tan\left(k_x^{(2)}d_2\right) + \epsilon_{r_2}k_x^{(1)}\tan\left(k_x^{(1)}d_1\right)\right]$$

$$N_{\mathrm{LSE}} = \tan\left(k_x^{(3)}d_3\right)\left[k_x^{(2)}\tan\left(k_x^{(1)}d_1\right) + k_x^{(1)}\tan\left(k_x^{(2)}d_2\right)\right]$$

$$D_{\mathrm{LSM}} = \epsilon_{r_2}k_x^{(3)}\tan\left(k_x^{(3)}d_3\right)\left[\epsilon_{r_2}k_x^{(1)}\tan\left(k_x^{(1)}d_1\right)\tan\left(k_x^{(2)}d_2\right) - \epsilon_{r_1}k_x^{(2)}\right] - k_x^{(2)}\left[\epsilon_{r_1}k_x^{(2)}\tan\left(k_x^{(2)}d_2\right) + \epsilon_{r_2}k_x^{(1)}\tan\left(k_x^{(1)}d_1\right)\right]$$

$$D_{\mathrm{LSE}} = k_x^{(3)}\left[k_x^{(2)}\tan\left(k_x^{(1)}d_1\right) + k_x^{(1)}\tan\left(k_x^{(2)}d_2\right)\right] + k_x^{(2)}\cdot\tan\left(k_x^{(3)}d_3\right)\left[k_x^{(1)} - k_x^{(2)}\tan\left(k_x^{(1)}d_1\right)\tan\left(k_x^{(2)}d_2\right)\right]$$

and

$$k_x^{(i)} = \sqrt{\omega^2\mu_0\epsilon_i - \left(\frac{m\pi}{b}\right)^2 - k_z^2}, \qquad i = 1,2,3.$$

References

[1] R. A. Pucel, "Design considerations for monolithic microwave circuits," *IEEE Trans. Microwave Theory Tech.*, vol. MTT-29, pp. 513–534, June 1981.

[2] R. S. Pengelly, "Hybrid vs. monolithic microwave circuits—A matter of cost," *Microwave Syst. News*, pp. 77–114, Jan. 1983.

[3] N. K. Das and D. M. Pozar, "A generalized spectral-domain Green's function for multilayer dielectric substrates with application to multilayer transmission lines," *IEEE Trans. Microwave Theory Tech.*, vol. MTT-35, pp. 326–335, Mar. 1987.

[4] L. Beyne and D. De Zutter, "Green's function for layered lossy media with special application to microstrip antennas," *IEEE Trans. Microwave Theory Tech.*, vol. 36, pp. 875–881, May 1988.

[5] T. Sphicopoulos, V. Theodoris, and F. Gardiol, "Dyadic Green's function for the electromagnetic field in multilayered isotropic media: An operator approach," *Proc. Inst. Elec. Eng.*, vol. 132, pt. H, no. 5, pp. 329–334, Aug. 1985.

[6] C. T. Tai, "Dyadic Green's function for a rectangular waveguide filled with two dielectrics," *J. Electromagnetic Waves and Appl.*, vol. 2, no. 3/4, pp. 245–253, 1988.

[7] L. P. Dunleavy and P. B. Katehi, "A generalized method for analyzing shielded thin microstrip discontinuities," *IEEE Trans. Microwave Theory Tech.*, vol. 36, pp. 1758–1766, Dec. 1988.

[8] L. Dunleavy and P. Katehi, "Shielding effects in microstrip discontinuities," *IEEE Trans. Microwave Theory Tech.*, vol. 36, pp. 1767–1774, Dec. 1988.

[9] P. B. Katehi and N. G. Alexopoulos, "Frequency-dependent characteristics of microstrip discontinuities in millimeter-wave integrated circuits," *IEEE Trans. Microwave Theory Tech.*, vol. MTT-33, pp. 1029–1035, Oct. 1985.

[10] R. W. Jackson and D. M. Pozar, "Full-wave analysis of microstrip open-end and gap discontinuities," *IEEE Trans. Microwave Theory Tech.*, vol. MTT-33, pp. 1036–1042, Oct. 1985.

[11] P. Kennis and L. Faucon, "Rigorous analysis of planar MIS transmission lines," *Electron. Lett.*, vol. 17, no. 13, pp. 454–456, June 1981.
[12] M. Aubourg, J. Villotte, F. Godon and Y. Garault, "Finite element analysis of lossy waveguides—Applications to microstrip lines on semiconductor substrate," *IEEE Trans. Microwave Theory Tech.*, vol. MTT-31, pp. 326–330, Apr. 1983.
[13] C. Krowne, "Slow-wave propagation in generalized cylindrical waveguides loaded with a semiconductor," *Int. J. Electron.*, vol. 58, no. 2, pp. 249–269, 1985.
[14] C. Tzuang and T. Itoh, "Finite-element analysis of slow-wave Schottky contact printed lines," *IEEE Trans. Microwave Theory Tech.*, vol. MTT-34, pp. 1483–1489, Dec. 1986.
[15] T. Mu and T. Itoh, "Characteristics of multiconductor, asymmetric, slow-wave microstrip transmission lines," *IEEE Trans. Microwave Theory Tech.*, vol. MTT-34, pp. 1471–1477, Dec. 1986.
[16] H. Hesegawa, M. Furukawa, and H. Yanai, "Properties of microstrip line on Si–SiO_2 system," *IEEE Trans. Microwave Theory Tech.*, vol. MTT-19, pp. 869–881, Nov. 1971.
[17] C. T. Tai, *Dyadic Green's Functions in Electromagnetic Theory*. Scranton, PA: Intext, 1971.
[18] R. Harrington, *Time Harmonic Electromagnetic Fields*. New York: McGraw-Hill, 1961.
[19] K. Gupta, R. Garg, and I. Bahl, *Microstrip Lines and Slotlines*. Norwood, MA: Artech House, 1979.
[20] E. Yamashita and K. Atsuki, "Analysis of microstrip-like transmission lines by nonuniform discretization of integral equations," *IEEE Trans. Microwave Theory Tech.*, vol. MTT-24, pp. 195–200, Apr. 1976.

✠

Thomas G. Livernois was born in Grosse Pointe, MI, on July 2, 1962. He received the B.S.E.E. degree (with honor) in 1984 from Michigan Technological University and the M.S.E.E. degree in 1986 from Michigan State University. Since September 1987, he has been working toward the Ph.D. degree in electrical engineering at the University of Michigan, Ann Arbor. His research interests are in the areas of integrated microwave circuits and dielectric waveguides.

From February 1987 to May 1989 he was an Instructor in electrical engineering at Lawrence Technological University, Southfield, MI.

Mr. Livernois is a member of the Engineering Society of Detroit, Lambda Chi Alpha, and an associate member of Sigma Xi.

✠

Pisti B. Katehi (S'81–M'84) received the B.S.E.E. degree from the National Technical University of Athens, Greece, in 1977 and the M.S.E.E. and Ph.D. degrees from the University of California, Los Angeles, in 1981 and 1984 respectively.

In September 1984 she joined the faculty of the EECS Department of the University of Michigan, Ann Arbor, as an Assistant Professor. Since then, she has been involved in the modeling and computer-aided design of millimeter-wave and near-millimeter-wave monolithic circuits and antennas.

In 1984 Dr. Katehi received the W. P. King Award and in 1985 the S. A. Schelkunoff Award from the Antennas and Propagation Society. In 1987 she received an NSF Presidential Young Investigator Award and a Young Scientist Fellowship awarded from URSI. Dr. Katehi is a member of IEEE AP-S, MTT-S and Sigma Xi.